Journal of Materials Chemistry B

Peroxidase Mimics of Platinum-Group Metals for in vitro Diagnostics: Opportunities and Challenges

Journal:	*Journal of Materials Chemistry B*
Manuscript ID	TB-PER-05-2023-001255.R1
Article Type:	Perspective
Date Submitted by the Author:	29-Jul-2023
Complete List of Authors:	Gao, Weiwei; University of Central Florida, Chemistry Eastwood, Hannah; University of Central Florida, Chemistry Xia, Xiaohu; University of Central Florida, Chemistry

Perspective to J. Mater. Chem. B

Peroxidase Mimics of Platinum-Group Metals for *in vitro* Diagnostics: Opportunities and Challenges

Weiwei Gao,[a] Hannah Eastwood,[a] and Xiaohu Xia*[a,b]

[a]*Department of Chemistry, University of Central Florida, Orlando, Florida 32816, United States;*

[b]*NanoScience Technology Center, University of Central Florida, Orlando, Florida 32816, United States.*

Corresponding author. E-mail: Xiaohu.Xia@ucf.edu

Abstract

Platinum-group metal (PGM) nanostructures with peroxidase-like catalytic activities (*i.e.*, peroxidase mimics) have been actively developed and applied to *in vitro* diagnostics in recent years. This article provides our viewpoints on this emerging field from the perspectives of materials science and solid-state chemistry angles. We start with an introduction to PGM peroxidase mimics, their catalytic efficiencies, and insights into catalysis from computational simulations. We then discuss chemical approaches to the synthesis of PGM peroxidase mimics with desired physicochemical parameters and catalytic properties. Then, we elaborate on general methods for functionalizing the surfaces of PGM mimics with bioreceptors. Thereafter, we highlight the applications of PGM mimics in *in vitro* diagnostics, emphasizing the interactions of PGM mimics with other components of a diagnostic system. We conclude this article with our opinions on the challenges and opportunities in this field.

Keywords:

Platinum-group metal; nanostructure; peroxidase mimic; catalysis; *in vitro* diagnostics

1. Introduction

Over the past few decades, nanostructures with peroxidase-like catalytic activities (*i.e.*, peroxidase mimics) have emerged as a class of functional materials for various biomedical applications, particularly in *in vitro* diagnostics.[1-4] In most diagnostic applications, peroxidase mimics are utilized in the same fashion as natural peroxidases (typically horseradish peroxidase, HRP[5,6]) that are widely used in commercially available diagnostic techniques, where peroxidases or mimics are functionalized with bioreceptors (*e.g.*, antibodies, nucleic acids, and avidin) and specifically produce a color signal by catalyzing chromogenic substrates (Figure 1).[1,7,8] Compared to natural peroxidases, the mimics are often more catalytically efficient and stable, offering sensitive and reliable diagnostics.[2,9] In a sense, specific diagnostic techniques can be advanced by simply substituting peroxidase mimics for natural peroxidases, without the need for additional materials, assay procedures and instruments.[10,11] Adopting existing assay platforms makes it convenient and straightforward to apply peroxidase mimics to diagnostic techniques. Such a practicability greatly motivates the rapid development of this niche field.

Since the first report of Fe_3O_4 nanoparticles as peroxidase mimics in 2007,[12] a wide variety of nanostructures made of different inorganic materials have been reported to possess peroxidase-like catalytic activities. Examples include nanomaterials of metals, metal oxides, carbons, and ceria.[13-20] Among various peroxidase mimics, platinum-group metal (PGM) nanostructures have drawn increasing interest in recent years owing to their superior properties. For instance, PGM nanostructures are more catalytically active than most other types of peroxidase mimics.[21,22] PGM nanostructures have exceptional resistance to oxidation and high temperatures, which contributes to their outstanding chemical and thermal stabilities. They can be conveniently functionalized with bioreceptors through noncovalent and/or covalent methods. Moreover, they can be synthesized in ordinary wet chemistry laboratories without the use of sophisticated instruments.[23] It is important to note that despite the high unit costs of PGMs, the materials cost of PGM peroxidase mimics is low in diagnostic applications because of the minimal usage amount (generally nanogram-level PGM per test, which is equivalent to < $1 per test based on the current prices of PGM).[24,25]

While numerous PGM nanostructures as peroxidase mimics have been developed, we do not intend to repeat and summarize what has been reported in this field. This perspective article aims to discuss fundamentally critical issues and practically useful viewpoints of PGM peroxidase mimics from the aspects of materials science and solid-state chemistry. We anticipate this article

will advance both the fundamental science and applied research of PGM peroxidase mimics.

2. Catalytic Efficiency and Insights from Computational Simulation

Since catalysis is the inherent driving force for peroxidase mimics to generate detection signals, catalytic efficiency is a key parameter that largely determines the performance of a peroxidase mimic in certain diagnostic applications. It should be emphasized that high catalytic efficiency is essential to ensuring a high sensitivity for related diagnostic techniques, particularly in detecting cancer and infectious diseases at preliminary stages.

The catalytic constant or turnover rate (K_{cat}), which is defined as the maximum number of substrate molecules converted to products per unit of time per catalyst, is used to quantify the catalytic efficiency of peroxidases or mimics.[1,21] K_{cat} can be experimentally determined through steady-state enzyme kinetics, where oxidation of 3,3',5,5'-tetramethylbenzidine (TMB, a typical peroxidase substrate[26,27]) by H_2O_2 is used as a model catalytic reaction and the Michaelis-Menten equation is applied to derive the kinetic parameters. Previous publications offer more information on how K_{cat} values are determined.[12,24] K_{cat} of horseradish peroxidase (HRP, the most commonly used natural peroxidase in diagnostics) as a benchmark for mimics is determined to be 4.3×10^3 s^{-1} towards TMB.[12,28] In comparison, K_{cat} values of peroxidase mimics with dimensions from 1 to 100 nm fall between a broad range of approximately $10^3 – 10^7$ s^{-1}.[1] It should be mentioned that sometimes a different unit of peroxidase mimic is used to ensure a clear or fair comparison of catalytic efficiencies between two different peroxidase mimics or a mimic and its natural counterpart. For instance, one could normalize K_{cat} against the surface area of an individual peroxidase mimic to derive the area-specific catalytic efficiency.[29] The catalytic efficiency could also be normalized based on the total number of surface atoms on a mimic.[30] Nevertheless, in the particular application of *in vitro* diagnostics (Figure 1), it is meaningful to compare catalytic efficiencies of peroxidase mimics in terms of K_{cat} values. A peroxidase mimic with a higher K_{cat} is expected to produce a stronger signal at a lower biomarker concentration within a specific amount of time, effectively enhancing the sensitivity of a diagnostic system.

PGM peroxidase mimics possess superior catalytic efficiencies compared to various types of other peroxidase mimics. For instance, in a recent study, we have demonstrated that Ir nanoparticles of only 3.61 nm (a similar dimension as HRP molecule) displayed a K_{cat} as high as 6.27×10^5 s^{-1}, which is two orders of magnitude greater than the K_{cat} of HRP.[31] The catalytic

mechanisms of PGM nanoparticles as peroxidase mimics (heterogeneous catalysts with multiple catalytic sites) and HRP as a natural enzyme (a homogeneous biological catalyst with a core catalytic site) are fundamentally different.[32] So far, the explicit catalytic mechanisms and kinetics of PGM peroxidase mimics have not been fully deciphered. The obstacles to mechanistic understanding primarily come from the transient intermediates on the nanostructure surface that are hard to be monitored and quantified in experiments.[33] Nevertheless, recent simulation studies based on density functional theory (DFT) calculations provide helpful insights into the micro-mechanisms and kinetics of PGM peroxidase mimics at the atomic level.[34] DFT as a quantum mechanical approach can be used to estimate thermochemical parameters (e.g., enthalpies and entropies) and kinetic parameters (e.g., activation energy) of chemical reaction systems.[35] DFT calculations simulate and predict reaction mechanisms and kinetics through analyses of the energy profiles and electronic structures along the reaction coordinates.[34,36,37] First-principles DFT provides the crucial energetic and structural accuracy needed to gain valuable insights into the catalytic processes mediated by PGM peroxidase mimics. Coupling DFT with chemical and materials theories, mathematical or stochastic modeling, and machine learning methods may allow its predictive power to be extended to achieve the simulation of reaction kinetics in complex interfacial environments. Taking Pd-based peroxidase mimics as an example, DFT calculations suggest that H_2O_2 can be decomposed on Pd surfaces to form reactive oxygen-containing adsorbates *via* steps: $H_2O_2^* \rightarrow 2OH^* \rightarrow H_2O^* + O^*$ (* denotes a surface-adsorbate species).[38] TMB is then oxidized by the surface absorbates, and the surfaces are subsequently recovered. Due to its high energy barrier, the homolytic cleavage of H_2O_2 is thought to be the rate-determining step. Significantly, DFT calculations can offer insights into structure- and composition-dependent catalytic efficiencies by building models using specific physicochemical parameters. More comprehensive discussions about DFT calculations for peroxidase mimics-mediated catalysis can be found in a recent review published elsewhere.[34]

3. Chemical Synthesis and Materials Design

In the application of *in vitro* diagnostics, most biological recognition processes (*e.g.*, interaction of bioreceptors with analytes) take place in aqueous media with specific pH values and ionic strengths. As such, PGM peroxidase mimics are expected to be water-dispersible. Solution-phase synthesis is often preferred to prepare PGM peroxidase mimics with good water dispersity.

A typical solution-phase synthesis of PGM peroxidase mimics involves the use of a solvent, a salt precursor to PGM, a reductant, and a colloidal stabilizer.[39] The reductant reduces salt precursor to produce metal atoms in a solvent that will nucleate and eventually form PGM nanostructures with colloidal stabilizers adhering to the surface. Frequently used solvents include water and polyols, with water being the most economical and sustainable solvent. In contrast, polyols are costly but more versatile.[40,41] Particularly, polyol can function as both a solvent and a reductant.[42] The reducing power of polyols can be manipulated by controlling the temperature and/or the hydrocarbon chain length.[43] To produce water-dispersible PGM peroxidase mimics, hydrophilic colloidal stabilizers (*e.g.*, citrate and polyvinylpyrrolidone) are introduced to the synthetic solution, which can bind to the mimic surfaces through chemisorption during synthesis.[44-46] The growth pathway of PGM nanocrystals and thus the morphology (*e.g.*, shape and size) of eventual mimics can be delicately controlled by adjusting various thermodynamic (*e.g.*, surface capping and reduction potential) and/or kinetic (*e.g.*, temperature and reagent concentrations) parameters of a synthetic system.[47-49] In addition to morphology, elemental composition of PGM peroxidase mimics can be controlled by introducing salt precursors of different metals to a synthesis. For multi-metallic systems, PGMs tend to form alloys when the reduction rates of different precursors are comparable. In contrast, core-shell structures may be formed if reduction rates of precursors are significantly different. Seed-mediated synthesis, in which a second metal is grown on preformed seeds, is another method for achieving composition-controlled synthesis.[50] More details about different synthetic methods for PGM nanocrystals using kinetic and thermodynamic approaches can be found in our previous publications.[47,50,51]

Catalytic efficiencies of PGM peroxidase mimics largely depend on their physicochemical parameters, such as shape, size, elemental composition, and strain. This relationship provides a strong foundation for the rational design of desired mimics. PGM peroxidase mimics normally have a face-centered-cubic (*fcc*) crystal structure.[39] Shape correlates to exposed facets on the PGM surface. Taking Pd-based peroxidase mimics as an example, it was found that Pd nanocubes covered by {100} facets were more catalytically efficient than Pd octahedra enclosed by {111} facets (Figure 2).[52] This is due to the fact that homolytic dissociation of H_2O_2 was easier on Pd(100) surface relative to Pd(111) surface; Size directly impacts the total surface area of a PGM mimic and thus its catalytic efficiency in terms of K_{cat} values. A larger-sized mimic tends to offer a higher K_{cat} due to the enlarged surface area. For instance, K_{cat} values of Pd-Ir nanoparticles increased from

9.4×10^4 to 1.2×10^6 s^{-1} as particle size increased from 3.3 to 13 nm.[29] Nevertheless, these nanoparticles displayed similar area-specific catalytic efficiencies; The elemental composition of PGM peroxidase mimics dictates their electronic structure and potential energy surface, which has a significant impact on their catalytic efficiency. For example, the peroxidase-like catalytic efficiency of Pt nanoparticles could be enhanced by up to ~40 times when it is coupled with Ni to form a Ni-Pt alloyed structure on the surface (Figure 3).[53] According to DFT calculations, Ni-Pt surfaces have a much weaker HO*/O* adsorption than Pt surfaces, which allows for a more facile oxidant species transfer to TMB substrate and, as a result, increased catalytic efficiency; Strain effect is known to play a crucial role in determining the catalytic activity of PGM nanocrystals in conventional heterogeneous catalysis. In a recent study, we have also demonstrated the strain effect in PGM peroxidase mimics using Pd as a model system.[54] The formation of OH radicals, a key intermediate for peroxidase mimics-mediated catalysis, was observed to benefit more from tensile strain than compressive strain. Collectively, it is important to be aware that the catalytic efficiency of PGM peroxidase mimics may be significantly changed when alternating physicochemical parameters.

4. Surface Functionalization

Prior to application in *in vitro* diagnostics, the surfaces of PGM peroxidase mimics are generally required to be functionalized with bioreceptors (*e.g.*, antibodies, avidins, and nucleic acids). Bioreceptors can be conjugated to PGM peroxidase mimics using non-covalent or covalent techniques. The following section discusses general conjugation techniques using antibodies as a model bioreceptor.

Non-covalent conjugation methods are based on electrostatic and/or hydrophobic interactions between antibody and PGM surfaces (Figure 4A).[55,56] Positively charged groups (*e.g.*, positively charged amino acids) are abundant in antibodies, which can bind to negatively charged PGM surfaces via electronic attraction. Hydrophobic interactions can take place through the adsorption between PGM surfaces and hydrophobic pockets on antibodies. In general, non-covalent conjugation is optimally achieved at a pH value close to the isoelectric point (pI) of the antibody to be conjugated.[57] At such a pH, electrically induced repulsive or attractive forces are neutralized, giving the antibody a net charge of zero.

Covalent methods are generally achieved through the covalent binding of PGM to free thiol

groups, which forms metal-thiol bonds (Figure 4B).[58,59] Linker molecules are frequently used as bridges in covalent techniques to attach antibodies to PGM peroxidase mimics. In terms of structure, a linker molecule has a thiol group (-SH) on one end and usually a carboxyl group (-COOH) on the other end.[24] The thiol end attaches to PGM surface *via* covalent bonding, while the carboxyl end couples to antibodies through chemical reactions. Through a condensation reaction, carboxylic groups can react with primary amines of antibodies to form amide bonds. For coupling of carboxyl and primary amine groups, the N-ethyl-N′-(3-(dimethylamino)propyl)carbodiimide (EDC)/N-hydroxysuccinimide (NHS) activation approach is generally utilized, which enables an efficient crosslinking without the addition of a spacer.[60,61] Thiol-polyethylene glycol-carboxyl (HS-PEG-COOH) is a type of commonly used linker for covalent conjugation of PGM peroxidase mimics and antibodies. The conjugates' solubility in water is increased by the hydrophilic nature of PEG the molecule. Additionally, by altering the PEG chain length, the distance between the PGM surface and the antibody can be tuned.

Both non-covalent and covalent techniques have advantages and disadvantages. In particular, non-covalent methods are easy-to-operate and cost-effective, which can be straightforwardly achieved through simple incubation of PGM mimics and bioreceptors without the involvement of extra chemicals and reagents. However, the resultant PGM mimic-bioreceptor conjugates may be unstable. Bioreceptors are non-covalently bound to PGM surfaces, therefore in some situations they can dissociate or be replaced by other molecules. Covalent techniques, on the other hand, result in more stable conjugates. A major disadvantage of covalent methods is that they often involve multiple steps of chemical reactions, which makes them inconvenient and costly.

Regardless of non-covalent or covalent methods, one should consider the possible reduction of catalytic efficiency of PGM mimics during conjugation. The catalytic efficiencies of PGM mimics are expected to decrease because bioreceptors on PGM occupy certain active sites on the surface. Nevertheless, peroxidase substrates (*e.g.*, H_2O_2 and TMB) are relatively small, so they can penetrate the bioreceptor layers and access the PGM surface. As a result, PGM mimics often retain some of their catalytic efficiency after conjugation with bioreceptors. However, if PGM surfaces are blocked by other small molecules (*e.g.*, linkers used in covalent conjugation), a significant reduction of catalytic efficiency will be observed. Along with surface accessibility, conjugation-related compositional and structural changes must be taken into consideration. For instance, when oxidative reagents are applied during conjugation, the oxidation state of surface PGM atoms and

the shape/size of PGM mimics may alter.

5. Applications in *in vitro* Diagnostics

PGM peroxidase mimics are normally used as signal transducers or labels in *in vitro* diagnostics.[1] In general, they provide color signals by catalyzing the oxidation of TMB by H_2O_2. They have been applied to various diagnostic platforms. Lateral flow assay (LFA) and enzyme-linked immunosorbent assay (ELISA) are two representative examples.[25,62-64] This section does not aim to summarize previously reported PGM peroxidase mimics-based diagnostics. The emphasis is instead on how to achieve a high detection sensitivity while maintaining a good specificity.

As shown in Figure 1, the detection signal originates from PGM mimics-medicated catalytic reaction. In principle, a more catalytically efficient PGM mimic is expected to yield a stronger signal and thus offer a higher detection sensitivity. The specificity of PGM labels is a crucial consideration in practical applications, along with catalytic efficiency, when assessing sensitivity. A poor specificity (*e.g.*, non-specific binding) will lead to a high background or a low signal-to-noise ratio (see Figure 5), and consequently compromised sensitivity. To enhance catalytic efficiencies of PGM mimics, one can carefully control their physicochemical parameters (see details in Section 3 above). Regarding specificity, the following factors may play critical roles. Firstly, good specificity of bioreceptors conjugated on PGM surfaces is the basis to ensure a specific capture of PGM mimics in a bioassay. Secondly, non-specific binding of PGM mimics to the materials used in a diagnostic system can cause non-specific signals (Figure 5). For instance, PGM mimics may bind to microplates in ELSIA or nitrocellulose membranes in LFA through physical or chemical adsorptions. A common strategy to eliminate such non-specific binding is to block PGM surfaces with non-specific proteins (*e.g.*, bovine serum albumin or ovalbumin). Thirdly, PGM mimics' morphology, particularly their size and shape, may affect how they interact with a diagnostic system. In LFA, for example, it was found that a larger-sized (*e.g.*, > 150 nm) PGM mimic migrated slowly in the nitrocellulose membrane.[63] The retention of mimics in the membrane could cause a significant background signal. It is worth noting that morphology can also impact the reactivity of PGM mimics. For instance, Pd-Ir nanoparticles of 3.3-13 nm as peroxidase mimics were used for the ELISA of a cancer biomarker.[29] Smaller nanoparticles were found to have greater diffusivities and reduced steric effect that make them more efficient to bind

to analytes during an assay, offering a higher sensitivity.

When a PGM mimic-based assay switches from detecting biomarker standards in buffers to testing clinical samples (*e.g.*, human blood and urine samples), it is frequently noticed that the background signal increases. In this case, the influence of complex matrices in biological samples should not be neglected. It is necessary to assess and rule out any potential non-specific binding of biological matrices to the surface of PGM mimics. Basically, the non-specific signal caused by matrices can be determined by comparing the tests in an assay buffer solution. To eliminate the non-specific binding of matrices to PGM mimics, two approaches can be applied. One is to use a washing buffer to remove the matrices from the assay system before adding PGM mimics. The alternative method is to modify PGM surfaces with hydrophilic molecules (*e.g.*, PEGs) that will make PGM mimics inert to the matrices.[65,66] In the event that the influence of matrices is severe, it is routine practice to dilute clinical samples with assay buffers prior to sample loading. In this case, dilution factors need to be considered when determining analytical performance (*e.g.*, quantification of detection limit).

6. Challenges and Perspectives

PGM peroxidase mimics can be employed in *in vitro* diagnostics in the same way that natural peroxidases are. As such, certain diagnostic techniques can be advanced by replacing peroxidases with PGM mimics. No additional materials, assay procedures, or instruments are required. This feature makes it convenient and practically feasible to use PGM mimics to upgrade existing diagnostic technologies. The enhanced performance of PGM mimics-based diagnostics relies on the higher catalytic efficiencies and superior stabilities of PGM mimics relative to natural peroxidases. Nevertheless, there are still challenges in this niche field.

It is difficult to produce PGM mimics consistently and with excellent batch-to-batch reproducibility. Contrary to natural peroxidases that have specific molecular structures, PGM mimics (even produced in the same batch of synthesis) exhibit various morphologies and structures at the atomic level. The structural disparity may lead to inconsistent performance in *in vitro* diagnostics, especially when a small amount of PGM mimics is captured in the assay. An effective strategy to mitigate inconsistent batch-to-batch production is to scale up the synthesis; The catalytic efficiency of certain PGM mimics has a strong dependence on the physicochemical parameters (*e.g.*, shape and elemental composition). In this regard, good stability of the PGM

mimic at the atomic level is critical to preserve its catalytic efficiency. It is important to assess PGM mimic stability while keeping track of structural and compositional alterations utilizing cutting-edge analytical instruments like high-performance electron microscopes; It is still challenging to retain the catalytic efficiency of PGM mimics while conjugating bioreceptors. After surface modifications, catalytically active sites on PGM surface may be taken up by bioreceptors. This problem might be resolved by site-selective conjugation after mapping the locations of active sites on the PGM surface; For the diagnostic applications discussed in this article, detection signal is color that is generated by PGM peroxidase mimics under specific conditions. In most cases, other enzyme-like activities of PGM nanocrystals do not influence the color signal and thus the diagnostic performance. However, without careful control of experimental conditions (e.g., pH value), the diagnostic application of PGM peroxidase mimics may be influenced by the multifunctional enzyme-like properties of PGM nanocrystals. For instance, PGM nanocrystals can act as catalase mimics (especially under alkaline conditions) to generate oxygen gas,[67,68] which may interference the absorbance reading of colorimetric signal; Fundamental studies on catalytic mechanisms and kinetics of PGM mimics deserve thorough investigations in the future. For instance, it is worth carefully studying the facet-dependent catalytic activity of PGM mimics. Although DFT calculations provide valuable insights into the catalytic mechanism of PGM peroxidase mimics-mediated catalytic reactions, understanding the catalytic mechanisms from experimental aspect is even more significant because experimental results offer direct evidence to support the assumptions. Some recent efforts from experimental angles have been made to capture and monitor key intermediates of catalytic reactions. For instance, electron spin resonance (ESR) analysis was performed to probe radicals (e.g., •OH and $O_2^{\bullet-}$),[69,70] and in situ Raman measurement was conducted to track intermediates absorbing on catalytic surfaces (e.g., atomic oxygen[71]); It is meaningful to explore new types of peroxidase mimics with superior catalytic activities and minimal usage of PGM materials. Recent studies on single-atom enzyme mimics represent a promising research direction;[72-75] PGM mimics-based diagnostic kits (*e.g.*, lateral flow tests) may be disposed of in the environment after use. Therefore, it is crucial to assess their impact on the environment and evaluate their biosafety. To this end, it is fundamentally important to understand the interactions of PGM mimics with biological and environmental media. Ultimately, we hope this article will inspire new fundamental studies and applied research in this emerging field.

Conflict of Interest

The authors declare no conflicts of interests.

Acknowledgments

This work was supported in part by grants from the National Science Foundation (CHE-1834874 and CEBT-1804525), the National Institute of Food and Agriculture, U.S. Department of Agriculture (2020-67021-31257), and startup funds from University of Central Florida (UCF).

References

1. Z. Wei, Z. Xi, S. Vlasov, J. Ayala and X. Xia, *ChemComm.*, 2020, **56**, 14962-14975.
2. J. Wu, X. Wang, Q. Wang, Z. Lou, S. Li, Y. Zhu, L. Qin and H. Wei, *Chem. Soc. Rev.*, 2019, **48**, 1004-1076.
3. C. Hong, X. Meng, J. He, K. Fan and X. Yan, *Particuology*, 2022, **71**, 90-107.
4. S. Li, Y. Zhang, Q. Wang, A. Lin and H. Wei, *Anal. Chem.*, 2021, **94**, 312-323.
5. N. C. Veitch, *Phytochem.*, 2004, **65**, 249-259.
6. S. Hiraga, K. Sasaki, H. Ito, Y. Ohashi and H. Matsui, *Plant Cell Physiol.*, 2001, **42**, 462-468.
7. R. M. Lequin, *Clin. Chem.*, 2005, **51**, 2415-2418.
8. R. Krieg and K. Halbhuber, *Cell. Mol. Biol. (Noisy-le-grand, France)*, 2003, **49**, 547-563.
9. M. Liang and X. Yan, *Acc. Chem. Res.*, 2019, **52**, 2190-2200.
10. A. Shamsabadi, T. Haghighi, S. Carvalho, L. C. Frenette and M. M. Stevens, *Adv. Mater.*, 2023, DOI: 10.1002/adma.202300184.
11. Y. Tang, Y. Chen, Y. Wu, W. Xu, Z. Luo, H.-R. Ye, W. Gu, W. Song, S. Guo and C. Zhu, *Nano Lett.*, 2022, **23**, 267-275.
12. L. Gao, J. Zhuang, L. Nie, J. Zhang, Y. Zhang, N. Gu, T. Wang, J. Feng, D. Yang and S. Perrett, *Nat. Nanotechnol.*, 2007, **2**, 577-583.
13. W. He, X. Wu, J. Liu, X. Hu, K. Zhang, S. Hou, W. Zhou and S. Xie, *Chem. Mater.*, 2010, **22**, 2988-2994.

14. W. He, Y. Liu, J. Yuan, J.-J. Yin, X. Wu, X. Hu, K. Zhang, J. Liu, C. Chen and Y. Ji, *Biomater.*, 2011, **32**, 1139-1147.
15. R. André, F. Natálio, M. Humanes, J. Leppin, K. Heinze, R. Wever, H. C. Schröder, W. E. Müller and W. Tremel, *Adv. Funct. Mater.*, 2011, **21**, 501-509.
16. X. Sun, S. Guo, C. S. Chung, W. Zhu and S. Sun, *Adv. Mater.*, 2013, **25**, 132-136.
17. M. Liu, H. Zhao, S. Chen, H. Yu and X. Quan, *ACS Nano*, 2012, **6**, 3142-3151.
18. Y. Song, K. Qu, C. Zhao, J. Ren and X. Qu, *Adv. Mater.*, 2010, **22**, 2206-2210.
19. K. M. Tripathi, H. T. Ahn, M. Chung, X. A. Le, D. Saini, A. Bhati, S. K. Sonkar, M. I. Kim and T. Kim, *ACS Biomater. Sci. Eng.*, 2020, **6**, 5527-5537.
20. Y. Jiang, Z. Ding, M. Gao, C. Chen, P. Ni, C. Zhang, B. Wang, G. Duan and Y. Lu, *Chin. J. Chem.*, 2021, **39**, 3369-3374.
21. H. Ye, Z. Xi, K. Magloire and X. Xia, *ChemNanoMat*, 2019, **5**, 860-868.
22. Y. Wang, T. Li and H. Wei, *Anal. Chem.*, 2023, **95**, 10105–10109
23. Y. Shi, Z. Lyu, M. Zhao, R. Chen, Q. N. Nguyen and Y. Xia, *Chem. Rev.*, 2020, **121**, 649-735.
24. X. Xia, J. Zhang, N. Lu, M. J. Kim, K. Ghale, Y. Xu, E. McKenzie, J. Liu and H. Ye, *ACS Nano*, 2015, **9**, 9994-10004.
25. H. Ye, K. Yang, J. Tao, Y. Liu, Q. Zhang, S. Habibi, Z. Nie and X. Xia, *ACS Nano*, 2017, **11**, 2052-2059.
26. A. K. Goka and M. J. Farthing, *J. Immunoassay.*, 1987, **8**, 29-41.
27. A. Frey, B. Meckelein, D. Externest and M. A. Schmidt, *J. Immunol. Methods*, 2000, **233**, 47-56.
28. H. Wei and E. Wang, *Chem. Soc. Rev.*, 2013, **42**, 6060-6093.
29. Z. Xi, W. Gao and X. Xia, *ChemBioChem*, 2020, **21**, 2440-2444.
30. M. Zandieh and J. Liu, *ACS Nano*, 2021, **15**, 15645-15655.
31. A. Biby, H. Crawford and X. Xia, *ACS Appl. Nano Mater.*, 2022, **5**, 17622-17631.
32. M. Zandieh and J. Liu, *Adv. Mater.*, 2023, 2211041.
33. S. Hu, C. Yang, Y. Li, Q. Luo and H. Luo, *Biosens. Bioelectron.*, 2022, **199**, 113881.
34. X. Shen, Z. Wang, X. J. Gao and X. Gao, *Adv. Mater.*, 2023, 2211151.
35. A. A. Gokhale, S. Kandoi, J. P. Greeley, M. Mavrikakis and J. A. Dumesic, *Chem. Eng. Sci.*, 2004, **59**, 4679-4691.

36. A. J. R. Hensley, K. Ghale, C. Rieg, T. Dang, E. Anderst, F. Studt, C. T. Campbell, J.-S. McEwen and Y. Xu, *J. Phy. Che. C*, 2017, **121**, 4937-4945.
37. C. A. Farberow, J. A. Dumesic and M. Mavrikakis, *ACS Catal.*, 2014, **4**, 3307-3319.
38. J. Li, W. Liu, X. Wu and X. Gao, *Biomater.*, 2015, **48**, 37-44.
39. Y. Xia, Y. Xiong, B. Lim and S. E. Skrabalak, *Angew. Chem. Int. Ed.*, 2009, **48**, 60-103.
40. H. Dong, Y.-C. Chen and C. Feldmann, *Green Chem.*, 2015, **17**, 4107-4132.
41. F. Fiévet, S. Ammar-Merah, R. Brayner, F. Chau, M. Giraud, F. Mammeri, J. Peron, J.-Y. Piquemal, L. Sicard and G. Viau, *Chem. Soc. Rev.*, 2018, **47**, 5187-5233.
42. S. E. Skrabalak, B. J. Wiley, M. Kim, E. V. Formo and Y. Xia, *Nano Lett.*, 2008, **8**, 2077-2081.
43. Y. Wang, H.-C. Peng, J. Liu, C. Z. Huang and Y. Xia, *Nano Lett.*, 2015, **15**, 1445-1450.
44. N. G. Bastús, J. Comenge and V. Puntes, *Langmuir*, 2011, **27**, 11098-11105.
45. X. Xia, J. Zeng, Q. Zhang, C. H. Moran and Y. Xia, *J. Phys. Chem. C*, 2012, **116**, 21647-21656.
46. H. Wang, X. Qiao, J. Chen, X. Wang and S. Ding, *Mater. Chem. Phys.*, 2005, **94**, 449-453.
47. Y. Xia, X. Xia and H.-C. Peng, *J. Am. Chem. Soc.*, 2015, **137**, 7947-7966.
48. X. Xia, S. Xie, M. Liu, H.-C. Peng, N. Lu, J. Wang, M. J. Kim and Y. Xia, *Proc. Natl. Acad. Sci. U.S.A.*, 2013, **110**, 6669-6673.
49. H. Ye, Q. Wang, M. Catalano, N. Lu, J. Vermeylen, M. J. Kim, Y. Liu, Y. Sun and X. Xia, *Nano Lett.*, 2016, **16**, 2812-2817.
50. Y. Xia, K. D. Gilroy, H. C. Peng and X. Xia, *Angew. Chem. Int. Ed.*, 2017, **56**, 60-95.
51. Z. Xi, H. Ye and X. Xia, *Chem. Mater.*, 2018, **30**, 8391-8414.
52. G. Fang, W. Li, X. Shen, J. M. Perez-Aguilar, Y. Chong, X. Gao, Z. Chai, C. Chen, C. Ge and R. Zhou, *Nat. Commun.*, 2018, **9**, 129.
53. Z. Xi, K. Wei, Q. Wang, M. J. Kim, S. Sun, V. Fung and X. Xia, *J. Am. Chem. Soc.*, 2021, **143**, 2660-2664.
54. Z. Xi, X. Cheng, Z. Gao, M. Wang, T. Cai, M. Muzzio, E. Davidson, O. Chen, Y. Jung, S. Sun, Y. Xu and X. Xia, *Nano Lett.*, 2019, **20**, 272-277.
55. M. H. Jazayeri, H. Amani, A. A. Pourfatollah, H. Pazoki-Toroudi and B. Sedighimoghaddam, *Sens. Bio-Sens. Res.*, 2016, **9**, 17-22.
56. R. G. Rayavarapu, W. Petersen, C. Ungureanu, J. N. Post, T. G. van Leeuwen and S. Manohar, *Int. J. Biomed. Imaging*, 2007, 29817.

57. W. Norde, *Adv. Colloid Interface Sci.*, 1986, **25**, 267-340.
58. Y. Xue, X. Li, H. Li and W. Zhang, *Nat. Commun.*, 2014, **5**, 4348.
59. M. S. Inkpen, Z. F. Liu, H. Li, L. M. Campos, J. B. Neaton and L. Venkataraman, *Nat. Chem.*, 2019, **11**, 351-358.
60. X. Qian, X.-H. Peng, D. O. Ansari, Q. Yin-Goen, G. Z. Chen, D. M. Shin, L. Yang, A. N. Young, M. D. Wang and S. Nie, *Nat. Biotechnol.*, 2008, **26**, 83-90.
61. A. Csáki, P. Kaplanek, R. Möller and W. Fritzsche, *Nanotechnology*, 2003, **14**, 1262.
62. Z. Wei, K. Luciano and X. Xia, *ACS Nano*, 2022, **16**, 21609-21617.
63. C. N. Loynachan, M. R. Thomas, E. R. Gray, D. A. Richards, J. Kim, B. S. Miller, J. C. Brookes, S. Agarwal, V. Chudasama and R. A. McKendry, *ACS Nano*, 2018, **12**, 279-288.
64. Z. Gao, M. Xu, L. Hou, G. Chen and D. Tang, *Anal. Chim. Acta*, 2013, **776**, 79-86.
65. J. S. Suk, Q. Xu, N. Kim, J. Hanes and L. M. Ensign, *Adv. Drug Deliv. Rev.*, 2016, **99**, 28-51.
66. L. Shi, J. Zhang, M. Zhao, S. Tang, X. Cheng, W. Zhang, W. Li, X. Liu, H. Peng and Q. Wang, *Nanoscale*, 2021, **13**, 10748-10764.
67. Z. Zhu, Z. Guan, S. Jia, Z. Lei, S. Lin, H. Zhang, Y. Ma, Z. Q. Tian and C. J. Yang, *Angew. Chem. Int. Ed.*, 2014, **53**, 12503-12507.
68. Y. Liu, H. Wu, M. Li, J.-J. Yin and Z. Nie, *Nanoscale*, 2014, **6**, 11904-11910.
69. C. Tang, T. Fang, S. Chen, D. Zhang, J. Yin and H. Wang, *J. Chem. Eng.*, 2023, **464**, 142726.
70. C. Ge, G. Fang, X. Shen, Y. Chong, W. G. Wamer, X. Gao, Z. Chai, C. Chen and J.-J. Yin, *ACS Nano*, 2016, **10**, 10436-10445.
71. Z. Wang, W. Wang, J. Wang, D. Wang, M. Liu, Q. Wu and H. Hu, *Adv. Funct. Mater.*, 2023, **33**, 2209560.
72. R. Yan, S. Sun, J. Yang, W. Long, J. Wang, X. Mu, Q. Li, W. Hao, S. Zhang and H. Liu, *ACS Nano*, 2019, **13**, 11552-11560.
73. W. Wu, L. Huang, E. Wang and S. Dong, *Chem. Sci.*, 2020, **11**, 9741-9756.
74. B. Jiang and M. Liang, *Chin. J. Chem.*, 2021, **39**, 174-180.
75. G. Li, H. Liu, T. Hu, F. Pu, J. Ren and X. Qu, *J. Am. Chem. Soc.*, 2023, DOI:10.1021/jacs.3c05162.

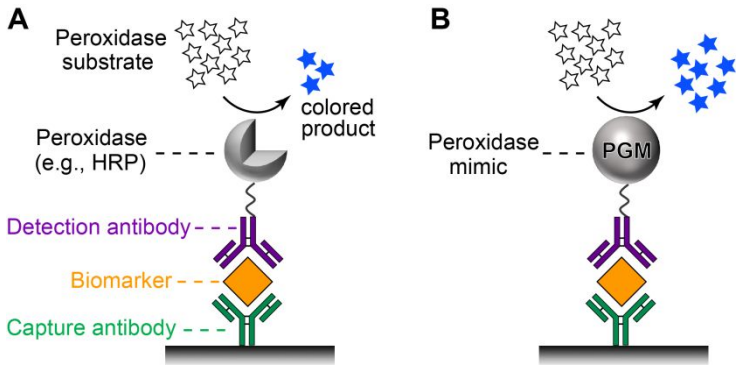

Figure 1. Natural peroxidase (A) *versus* platinum-group metal (PGM) peroxidase mimic (B) in a typical assay (*e.g.*, enzyme-linked immunosorbent assay, ELISA) of biomarkers. An individual peroxidase mimic can generate more colored products (blue stars) than an individual natural peroxidase.

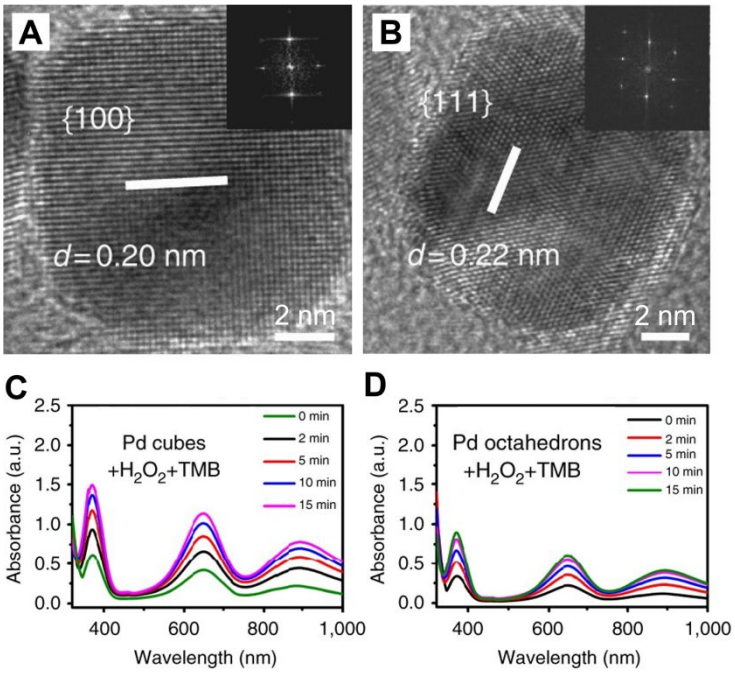

Figure 2. Comparison of peroxidase-like catalytic efficiencies of Pd nanocubes and octahedrons. (A, B) High-resolution transmission electron microscopy (HR-TEM) images of a Pd nanocube (A) and a Pd octahedron (B). (C, D) Time-dependent absorbance spectra of reaction solutions containing TMB and H_2O_2, which were catalyzed by Pd nanocubes (C) and Pd octahedrons (D). Adapted with permission from ref. 52. Copyright 2018 Nature Portfolio.

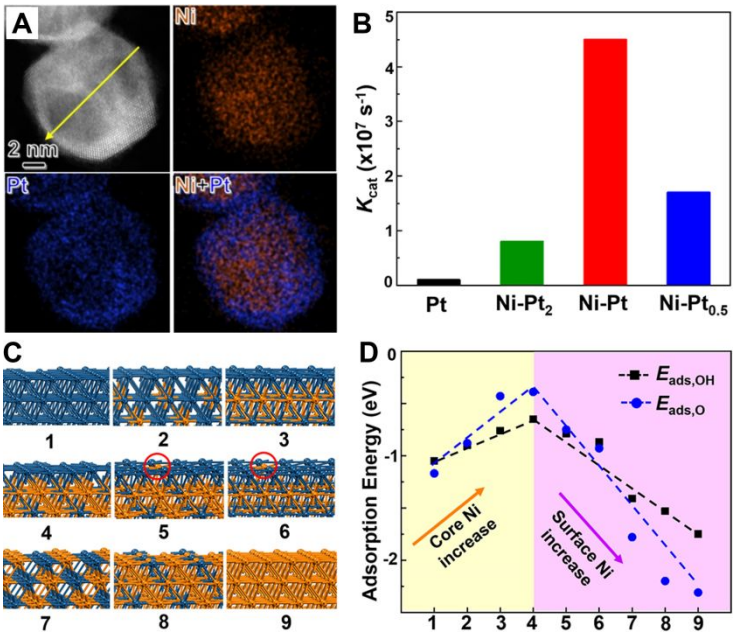

Figure 3. Peroxidase-like catalytic efficiencies of Ni-Pt nanoparticles with Ni-rich cores and Pt-rich shells. (A) Scanning TEM image and energy dispersive spectrometry (EDS) mapping images of a single nanoparticle. (B) Histograms comparing K_{cat} values of various nanoparticles with different atomic ratios of Ni to Pt. (C, D) DFT calculations: (C) Slab models for various NiPt surfaces, and (D) Adsorption energies for OH and O on the NiPt slab model surfaces in (C). In the slab models, blue and orange atoms represent Pt and Ni, respectively. Reprinted with permission from ref. 53. Copyright 2021 American Chemical Society.

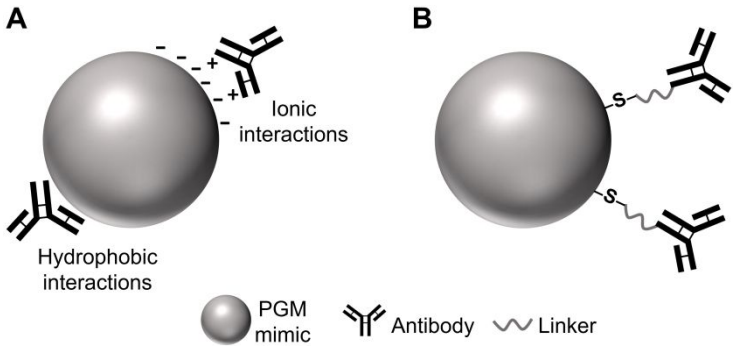

Figure 4. Schematics showing: (A) non-covalent method and (B) covalent method for conjugating PGM peroxidase mimics with antibodies.

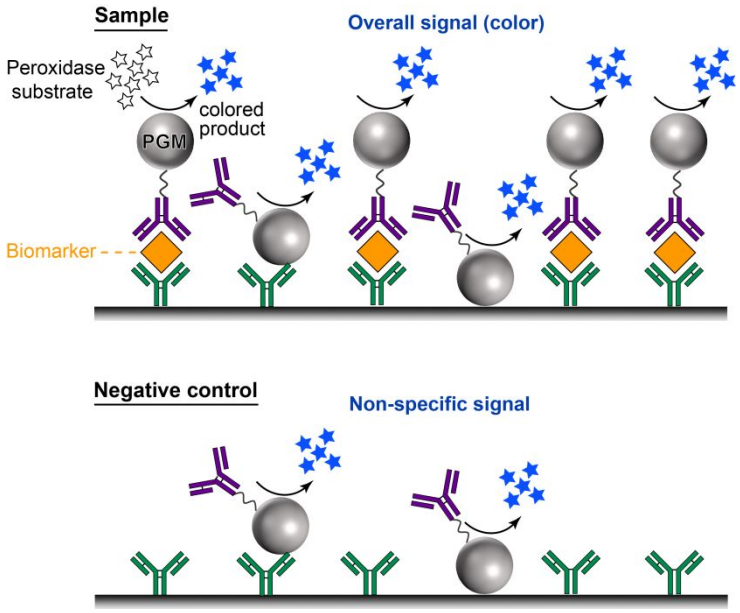

Figure 5. Schematics showing the detection of a positive sample (with biomarker) and negative control (without biomarker) by PGM peroxidase mimic-based assay. Highlighted are the non-specific signal caused by the non-specific binding of PGM peroxidase mimics to the assay system.